Controlled Capacitive Gaps for Electrostatic Actuation and Tuning of 3D Fused Quartz Micro Wineglass Resonator Gyroscope

Mohammad H. Asadian, Yusheng Wang, Sina Askari and Andrei Shkel
MicroSystems Laboratory, University of California, Irvine, CA, USA
Email: {asadianm, yushengw, sina.askari, andrei.shkel} @ uci.edu

***Abstract*—In this paper, we present the assembly process and an electrostatic actuation, detection, and tuning method of micro-glassblown wineglass resonators using an out-of-plane electrode architecture with controlled uniform capacitive gaps. This process is developed based on wafer-level deposition of a sacrificial layer on planar electrodes wafer to achieve a uniform electrostatic gap (<5μm). The materials, bonding type, etch selectivity, temperature and vacuum compatibility of the process are considered in the assembly process of the micro-glassblown fused quartz shell resonators. Tuning the frequency mismatch between two orthogonal (n=2) in-plane wineglass modes is demonstrated experimentally on a 7 mm micro-glassblown wineglass resonator using the out-of-plane electrodes. An open-loop rate response is demonstrated using out-of-plane capacitive actuation and detection. The proposed process enables a low-cost assembly with a high transduction efficiency toward wafer-scale fabrication of micro 3D wineglass gyroscopes.**

***Keywords*—fused quartz; electrostatic tuning; assembly; micro-glassblowing; 3D wineglass resonator; capacitive gap**

I. Introduction

3D MEMS is an area of interest for the development of micro-scale high-performance sensors for inertial navigation applications. The micro-glassblowing process was proposed in [1] to fabricate 3D inverted micro-wineglass resonators out of low internal loss materials, such as Fused Quartz and Ultra Low Expansion Titania Silicate Glass (ULE TSG). The initial characterization results of a micro-glassblown 3D fused quartz resonator were reported at JMEMS 2015, [2]. Blow torch-molding was proposed as an alternative approach to fabricate 3D fused quartz shell resonators, [3]. An energy decay time of 130 seconds was reported in [4], demonstrating the potential of the micro-scale 3D shell to achieve the high-performance gyroscope operation.

Unlike conventional Silicon MEMS fabrication, in which the electrodes are co-fabricated with the sensing elements and capacitive gaps are defined by the high aspect ratio DRIE process, our current approach for 3D micro shell device fabrication requires an additional assembly step to integrate the 3D shells with actuation and detection electrodes. One of the challenges in the assembly of micro shell devices is achieving a uniform gap with efficient transduction. On macro-scale, spherical electrodes are machined and precisely assembled on HRGs to make 3D radial capacitive gaps [5]. An alternative approach is proposed by SAGEM [6], where a planar electrode configuration was utilized to makes capacitive gaps to actuate and detect the axial displacement of the rim of the shell. The planar electrode configuration was adapted for electrostatic actuation and detection of micro-glassblown wineglass shells and a wafer-level assembly process was proposed in [7]. Utilization of the planar electrodes make the assembly process less complicated, cost-effective, and accommodating to the small off-center error as compared to the radial electrode arrangement.

In this paper, a complete assembly process is presented to reduce the capacitive gaps to smaller than 5μm and obtain a higher efficiency for the actuation, detection, and the frequency mismatch tuning. The proposed process also considers the temperature and high-vacuum compatibility of the materials being used in the assembly of micro shell resonators.

This material is based on work supported by the Defense Advanced Research Projects Agency under Grant W31P4Q-11-1-0006.

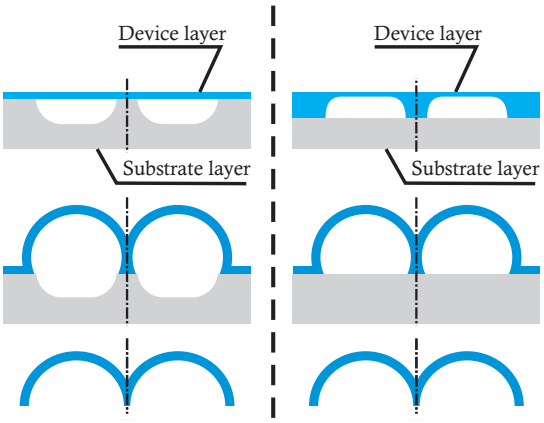

Fig. 1. Micro-wineglass fabrication process; (left) device layer bonded to the pre-etched cavities, (right) pre-etched device layer bonded to a flat substrate (this work).

II. Fused silica micro-glassblown wineglass resonator

In the micro-glassblowing process, a fused quartz substrate wafer is initially coated with a thin film of LPCVD PolySilicon (2μm) as a hard mask for etching. Cavities are etched in the wafer using 48% Hydrofluoric acid (HF) wet etching. After removing the hard mask, a blank fused quartz wafer is bonded to the pre-etched wafer using plasma-assisted fusion bonding. This creates encapsulated and hermetically sealed cavities. Heating up the bonded pairs of wafers above the softening point of the fused quartz (>1700 °C) causes (1) expansion of the trapped air inside the enclosed cavities and (2) viscous flow of the device layer due to combination of high temperature and high-pressure effects, creates a 3D axisymmetric geometry with self-aligned stem. The fabrication process of fused quartz shell resonators is shown in Figure 1.

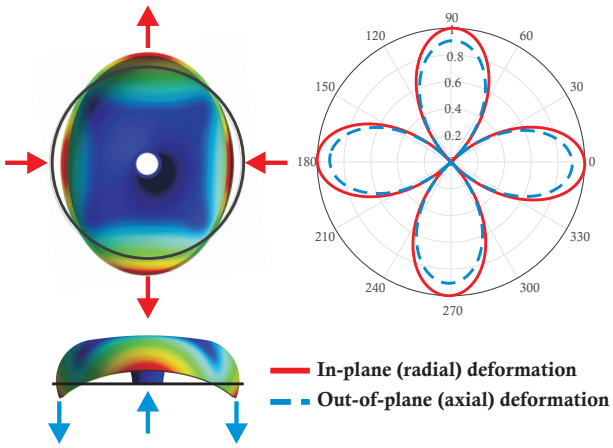

Fig. 2. In-plane (red) and out-of-plane components of a wineglass shell resonator. The ratio of out-of-plane to in-plane amplitude is approximately 0.9 on a 7 mm shell with $\sim$110μm thickness

Two variations of the process are illustrated; in the baseline process the device layer is bonded to a pre-etched substrate layer, and in the modified process the pre-etched device layer is bonded to a flat substrate wafer. A combination of the processes enables the fabrication of shell resonators with a wide range of operational frequencies, from 5 kHz to 300 kHz. 3D micro shells are released by parallel back-lapping of the substrate wafer followed by fine-polishing using diamond films and polishing cloths.

III. Electromechanical Modeling of Frequency Tuning Using Out-of-Plane Electrodes

The mode shape of a 3D shell resonator in its wineglass modes of vibration has three components: in-plane radial, tangential, and an out-of-plane axial displacement. The ratio of the amplitude of axial to radial component depends on the geometry of the shell. In hemi-toroidal micro-glassblown shell resonators, with a radius-to-height ratio of around 2, the out-of-plane to in-plane displacement ratio is $>$ 3:4 [7]. Figure 2 shows the 3D mode shape of a micro shell resonator. For the device under test in this work, 7 mm in diameter with $\sim$110μm in thickness, the normalized radial and axial displacement of the rim vibrating in (n=2) wineglass mode revealed the

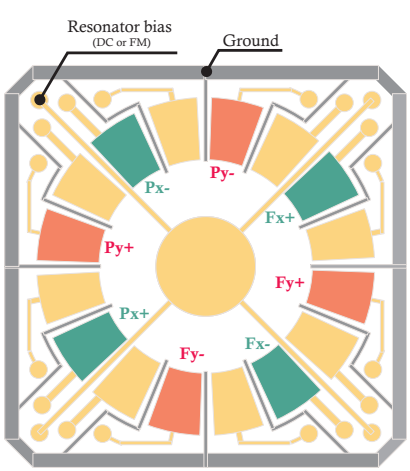

Fig. 3. The electrode configuration for differential excitation and detection of wineglass modes, green (Fx+. Fx-, Px+, Px-) and red (Fy+. Fy-, Py+, Py-) indicate excitation and detection electrodes for X and Y-mode, respectively.

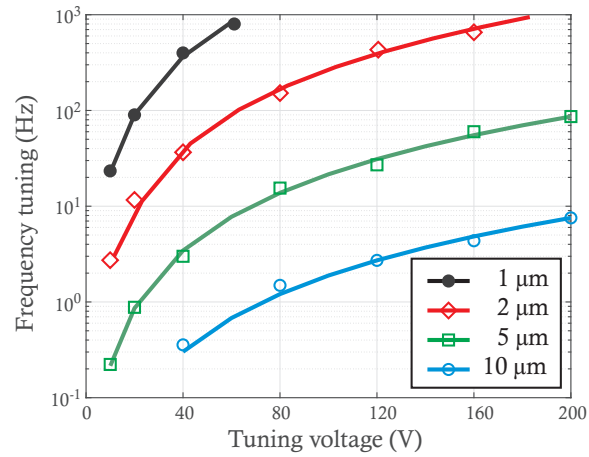

Fig. 4. Finite element simulation results of the electrostatic frequency tuning of a 17 kHz shell resonator with different capacitive gaps and tuning bias. The results suggests using gap $<$5μm for tuning capabilities.

amplitude ratio close to 1:1. Although the axial displacement component is not directly sensitive to the Coriolis force from the z-axis rotation, it can be utilized to actuate the in-plane vibration of 3D shell and detect the Coriolis-induced amplitude along the sense direction.

The efficiency of parallel plate capacitive transduction is approximately proportional to the overlapped surface area divided by the square of the gap. The overlapped area is limited by the thickness of shell at the rim, therefore the capacitive gaps must be designed for efficient transduction and to compensate for the surface area. The effect of capacitive gap size on the electrostatic frequency tuning was simulated using a coupled electromechanical model. A schematics of the electrodes configuration used in this work is illustrated in Figure 3. The 16 discrete electrodes were utilized for n=2 wineglass mode operation of micro shells. Two orthogonal pairs of electrodes were designated for actuation and detection of each mode. The in-between electrodes were designated for mode decoupling in the presence of mode-to-electrode misalignment. In the modeling, it was assumed that electrodes are perfectly aligned with the wineglass modes and DC tuning voltage was applied only to the drive electrodes. The electrostatic frequency tuning results using out-of-plane electrodes at different capacitive gaps on a 17 kHz shell are shows in Figure 4. Smaller gaps would relax the voltage requirements as the negative electrostatic spring is inversely proportional to the capacitive gap cubed. Therefore, reducing the capacitive gap can dramatically increase the frequency tuning efficiency.

IV. Assembly and Integration of 3D Fused Quartz Resonators

A schematics of the assembly process of micro-glassblown wineglass resonators to form a uniform out-of-plane capacitive gap is illustrated in Figure 5. This process includes: (1) patterning gold electrodes and traces on a fused quartz wafer, (2) selective deposition of a sacrificial layer, (3) shell-to-electrode attachment, and (4) removing the sacrificial layer and releasing the shell. Three main goals were pursued in the development of the assembly process: (1) vacuum compatibility in material selection for assembly and packaging, (2) compatibility of the materials with the temperature of thermo-compression bonding

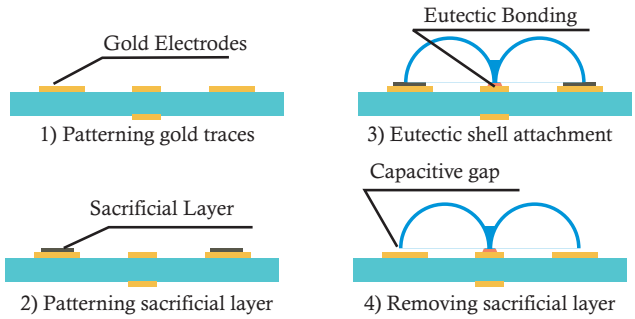

Fig. 5. The developed assembly process for capacitive gap definition between out-of-plane electrodes and Fused Quartz shell.

and vacuum sealing, (3) achieving capacitive gaps smaller than 5μm based on the results of electromechanical simulations.

A. Electrode substrate and capacitive gap definition

The planar electrodes and traces were defined on a fused quartz substrate wafer by deposition and patterning of thin film Cr/Au layers. The planar discrete electrodes for actuation, tuning, and detection, a central contact pad, and metal traces were designed for both electrical biasing and mechanical anchoring the shell. A sacrificial layer up to 5 μm in thickness was selectively formed on gold traces. The thickness of the layer, compatibility of the material with the subsequent shell-to-electrode attachment temperature (for example, $\sim$ 300°C for AuSn (80-20) eutectic bonding), and scalability on the wafer-level were considered for this step. Table I summarizes the trade-offs of the material selection. A thin film Nickel layer was electroplated prior to shell attachment as the sacrificial layer.

B. Attachment of fused quartz shell to substrate of electrodes

Shell resonators were attached to the electrodes substrates through their central stem. The central stem acts as a mechanical anchor point as well as an electrical connection for biasing the shell. This imposes electrical conductivity requirement for the shell attachment. In addition, the material has to be low out-gassing, compatible with the temperature of the subsequent vacuum sealing process (maximum temperature of 320°C), and provide high bond strength. Table II summarizes the process requirements and different types of attachments which were explored in this work.

Low melting temperature of Indium alloy, out-gassing of die attachment epoxies (JM7000 and 84-1LMI) after vacuum sealing, and dielectric properties of glass frit do not meet the process requirements. An alternative bonding method to attach shell resonators to electrode substrate is Gold-Tin (80/20) alloy eutectic bonding. To perform the bonding, the inner surface of fused quartz shell resonators was coated with Cr/Au. A stack of electrode substrate-AuSn preform-wineglass was heated up to above the eutectic point inside a vacuum reflow chamber. This technique provides a low out-gassing and a strong bond between shell and electrode substrate.

TABLE I. SACRIFICIAL LAYER MATERIAL SELECTION

Sacrificial layer	Implementation	Remarks	Results
Shim	Manual	- Limited to 10 μm thickness - Compatible w/ AuSn process	Large gaps
Photo-resist	Spin-coating	- Uniform, wafer-level - Not compatible w/ AuSn process	Not applicable
Thin film Nickel	Electro-plating	- Uniform, wafer-level - Compatible w/ AuSn process	<5μm gaps

TABLE II. MATERIAL SELECTION COMPATIBILITY AND THE PROCESS REQUIREMENTS FOR SHELL TO ELECTRODE ATTACHMENT PROCESS

Bonding type	Temp. compatibility	Outgassing	Conductivity	Strength
Glass Frit	Yes	Yes	No	Yes
Indium alloy	No	No	Yes	No
Epoxy	Yes	No	Yes	No
Eutectic	Yes	Yes	Yes	Yes

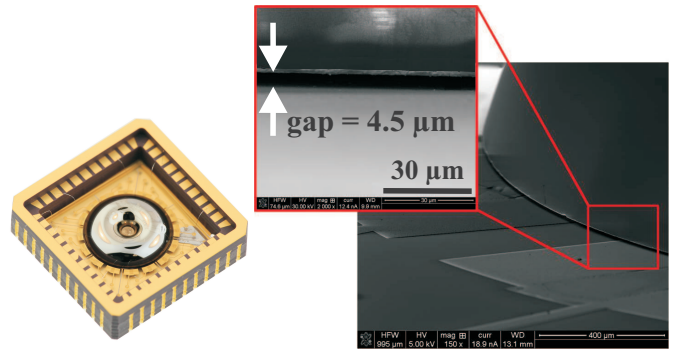

Fig. 6. An assembled and packaged device (left), SEM image of the capacitive gap (right), inset figure shows 4.5 μm gap size measurement.

C. Controlled small capacitive gaps

After the attachment step, the sacrificial layer was etched away to form the capacitive gaps. A compatible Nickel etchant TFG was used to selectively remove the Ni sacrificial layer without damaging Cr/Au electrodes and fused quartz. Figure 6 shows an assembled and packaged fused quartz device and an SEM image of the capacitive gap between the rim of the shell and the planar electrodes, demonstrating uniform <5μm capacitive gaps. The measured total rest capacitance of the assembled devices are presented in Table III. The total capacitance of a device assembled using Ni thin film sacrificial layer was as high as $\sim$14 pF, which experimentally confirms a reduction in the gap size.

TABLE III. CAPACITANCE MEASUREMENT OF THE ASSEMBLED DEVICES

Device No.	Sacrificial layer	Capacitive gap [μm]	Rim thickness [μm]	Total capacitance [pF]
1	Thin film Ni	$\sim$5	110	9.6
2	Thin film Ni	$\sim$5	175	14
3	Thin film Ni	$\sim$5	150	11
4	10 μm shim	$\sim$12	150	5.6
5	10 μm shim	$\sim$12	150	5.7
6	25 μm shim	$\sim$25	500	7.9
7	25 μm shim	$\sim$25	500	7.9

V. EXPERIMENTAL RESULTS

A. Electrostatic frequency tuning

The planar gold electrodes and the rim of shell create parallel-plate type actuation and detection electrodes. The

electrostatic spring softening acting on the axial component of the shell oscillation indirectly acts upon the in-plane frequency tuning. Figure 7 illustrates the frequency sweep response of the assembled fused quartz shell with different tuning voltages (V_t). The mismatch between the modes was tuned electrostatically from 7 Hz (as-fabricated) to $<$ 100 mHz by applying DC tuning up to 58 V, which is in close agreement with the FEA results.

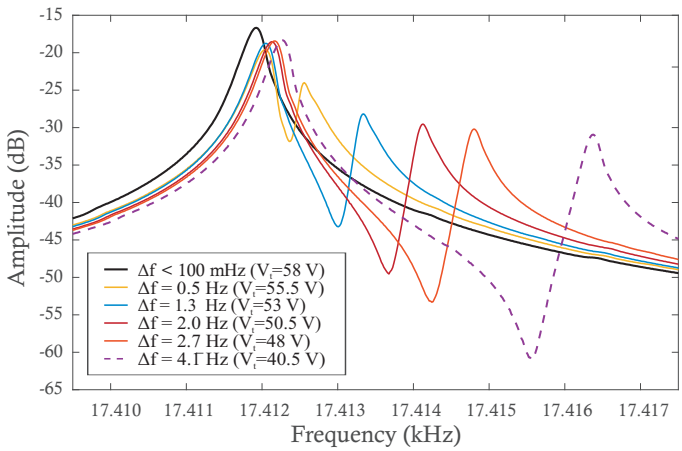

Fig. 7. Experimental results on electrostatic tuning of n=2 in-plane wineglass modes using out-of-plane electrodes with 4.5 μm capacitive gaps, 58 V tuning voltage was required for tuning the as-fabricated df of 7 Hz to $<$100 mHz at 17.4 kHz center frequency (device no. 1 in Table III).

B. Open-loop rate response

An open-loop rate response of the assembled fused quartz micro-wineglass gyroscope was characterized by applying a sinusoidal input rotation at different input rates on a rate-table. Figure 8 shows the output of the device with respect to input angular rotations. A scale factor of 0.49 mV/(deg/sec) was extracted using Phase-Locked Loop (PLL) and Amplitude Gain Control (AGC) loops on the drive mode without any frequency tuning and quadrature compensation. This is our first demonstration of gyro operation on an assembled fused quartz micro shells with the out-of-plane electrode architecture.

VI. Conclusion

An assembly process developed to integrate micro-glassblown wineglass resonators with planar electrodes. This process enabled to achieve a uniform capacitive gap with an effective transduction for actuation, detection, and electrostatic frequency tuning. A capacitive gap $<$5μm (1:20 aspect rate) was demonstrated on 7 mm fused quartz shell resonators, forming the total active capacitance of up to 14 pF for electrostatic operation. For the first time, rate response of a vacuum sealed fused quartz gyroscope operating in open-loop mode was demonstrated experimentally. The proposed assembly process showed an accurate control over the definition of capacitive gaps, which is critical for tuning and controlling the vibration shape for the rate and rate-integrating modes of operation. The high-vacuum and high-temperature (up to 300°C) compatibility of the materials and the processes allow for vacuum sealing of the assembled devices with getter activation, which is an important step toward the operation of high-performance 3D micro wineglass gyroscopes.

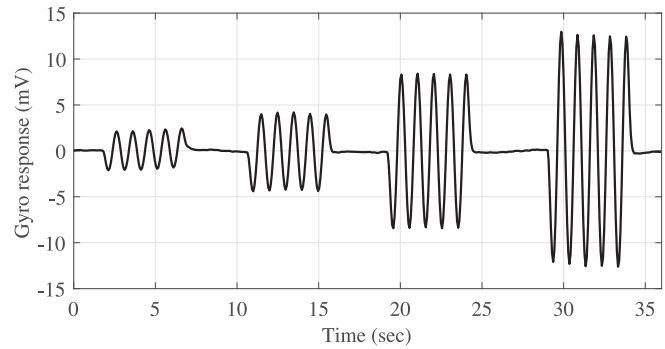

Fig. 8. Open-loop rate response of a micro-glassblown fused quartz gyroscope (device no. 1 in Table III) under $\pm$ 5, 10, 20, and 30 (deg/sec) sinusoidal input rate, revealing an open-loop scale factor of 0.49 mV/(deg/sec).

Acknowledgment

Design and characterization was done in UCI Microsystems Lab. Fabrication was done at UCI INRF facility. Authors would like to acknowledge Dogukan Yildirim, Yu-Wei Lin, and Radwan Noor for their help in thin film processes.

References

[1] D. Senkal, M. Ahamed, A. Trusov, and A. Shkel, "High temperature micro-glassblowing process demonstrated on fused quartz and ULE TSG," *Sensors and Actuators A: Physical*, vol. 201, pp. 525–531, 2013.

[2] D. Senkal, M. J. Ahamed, M. H. Asadian, S. Askari, and A. M. Shkel, "Demonstration of 1 Million Q-Factor on Microglassblown Wineglass Resonators With Out-of-Plane Electrostatic Transduction," *IEEE Journal of Microelectromechanical Systems*, vol. 24, no. 1, pp. 29–37, 2015.

[3] J. Y. Cho, J. Yan, J. A. Gregory, H. W. Eberhart, R. L. Peterson, and K. Najafi, "3-dimensional blow torch-molding of fused silica microstructures," *IEEE Journal of Microelectromechanical Systems*, vol. 22, no. 6, pp. 1276–1284, 2013.

[4] T. Nagourney, J. Y. Cho, A. Darvishian, B. Shiari, and K. Najafi, "130 Second Ring-Down Time and 3.98 Million Quality Factor in 10 kHz Fused Silica Micro Birdbath Shell Resonator," in *Solid-State Sensors, Actuators, and Microsystems Workshop*, Hilton Head Island, SC, USA, June 5-9 2016.

[5] D. M. Rozelle, "The hemispherical resonator gyro: From wineglass to the planets," in *Proc. 19th AAS/AIAA Space Flight Mechanics Meeting*, Savannah, Georgia, USA, February 8-12 2009.

[6] A. Jeanroy and P. Leger, "Gyroscopic sensor and rotation measurement apparatus constituting an application thereof," Nov. 5 2002, uS Patent 6,474,161.

[7] D. Senkal, M. J. Ahamed, M. H. Asadian, S. Askari, and A. M. Shkel, "Out-of-plane electrode architecture for fused silica micro-glassblown 3-D wineglass resonators," in *IEEE Sensors Conference*, Valencia, Spain, November 2-5 2014.